atoms

MDPI

Article

Electron Impact Ionization of Adenine: Partial Cross Sections

Mohammad Atiqur Rehman [1] and E. Krishnakumar [2,*]

[1] Tata Institute of Fundamental Research, Homi Bhabha Road, Colaba, Mumbai 400005, India
[2] Raman Research Institute, C V Raman Avenue, Sadashiva Nagar, Bangalore 560080, India
* Correspondence: ekkumar@tifr.res.in

Abstract: Electron ionization of a genetically important nucleobase, adenine, was investigated from threshold to 500 eV using crossed electron beam–effusive molecular beam geometry and time-of-flight mass spectrometry. We measured the complete set of absolute partial cross sections for adenine using the relative flow technique (RFT) up to an electron energy of 500 eV. Normalization to absolute values was performed using electron ionization cross sections for argon and the vapor pressure data of adenine. The total cross sections obtained by summing the partial cross sections were compared with the existing theoretical and experimental data. The appearance energies of various fragment ions were also measured and compared with the reported data. The prominence of ions with mass $(HCN)_n^+$ (n = 1 to 5) indicated a possible pathway to form adenine in the interstellar medium through aggregation of HCN units. Analysis of the partial cross sections for various groups of fragment ions as a function of electron energy was found to give insights into their composition.

Keywords: electron ionization; absolute cross sections; molecular processes—ISM: molecules

check for updates

Citation: Rehman, M.A.; Krishnakumar, E. Electron Impact Ionization of Adenine: Partial Cross Sections. *Atoms* **2022**, *10*, 100. https://doi.org/10.3390/atoms10040100

Academic Editor: David D. Reid

Received: 30 August 2022
Accepted: 18 September 2022
Published: 23 September 2022

1. Introduction

Measurement of absolute total and partial cross sections for electron-impact ionization of biological molecules is important in radiation biology. Any high energy radiation on interaction with matter in a condensed form leaves a final trail of low energy electrons [1,2]. These electrons are produced through a cascade of ionization processes. Thus, the large number of secondary electrons and ions produced in the process carry a dominant fraction of the energy of the incident radiation [2,3]. In biological matter, these charge particles can interact resonantly or directly with the biomolecules through a series of reactions, causing damage to the DNA and the RNA in terms of either single or double strand breaks [3–5]. The direct interaction can break the backbone of the DNA, while the resonances or transient anion formation will create neutral radicals and anionic fragments [1–5]. Thus, to understand the radiation damage and its complete description, the entire sequence of events leading to the final chemical state of the molecules must be known, and the mechanisms involved must be understood. The complete set of absolute cross sections resulting from low to intermediate energy electron collisions with DNA molecules and its building blocks are needed as input in bio-chemical models as well as in Monte Carlo particle track simulations used to study damage in living cells induced by ionizing radiations, nano- and micro-dosimetry, and cancer therapy [6–9]. Monte Carlo track simulations [6] of radiation damage accounts for ionization, but the probability of simultaneous ionization and dissociation, known as dissociative ionization, has not been incorporated in these simulations or in any other model due to the unavailability of either theoretical or measured data on such processes for DNA bases. These data are in the form of partial cross sections, which are the cross sections for the formation of an ion of specific mass-to-charge ratio. Despite its importance, very limited data on the absolute partial ionization cross sections of the DNA bases exist though absolute total ion cross sections for the DNA and RNA bases up to 200 eV have been reported [10–13]. In recent works on adenine ionization, Minaev et al. [11] studied the formation of positive and negative ions of adenine under

the impact of electrons (from 0.1 to 200 eV) using the crossed electron and molecular beam technique. The method measures the molecular beam intensity and determines the total cross sections for the formation of positive and negative ions of the studied molecules, their energy dependences, and absolute values. Quantum chemical calculations are performed for the studied molecules, ions, and fragments for interpretation of the crossed beams experiments. Jochims et al. [14] used photoionization mass spectrometry with synchrotron radiation in the 6–22 eV photon energy range to investigate fragmentation pathways, ionization energies, and ion appearance energies (AEs) and compared them with the results of electron impact. Dawley et al. [15] investigated the electron ionization of adenine near the threshold region using a high-resolution hemispherical electron monochromator and a quadrupole mass spectrometer. Ion efficiency curves of the threshold regions and the corresponding appearance energies (AEs) are presented for the parent cations and the five most abundant fragment cations of each molecule. The enthalpies of the possible reactions from the adenine were also obtained computationally, and ionization energies were calculated using quantum chemical calculations. van der Burgt et al. [16] measured the mass spectra, the relative ion yield, and appearance energies for various fragment ions up to 100 eV. They obtained the partial cross sections after normalizing their data to the theoretical values of total ion cross sections. Very recently, Ostroverkh et al. [17] measured the mass spectrum at 70 eV in a crossed beam experiment and the ion yield curves near the threshold.

On the theoretical side, there have been several reports on the total ionization cross sections. These include those using semi-classical Deutsch-Märk formalism and Binary-Encounter Bethe (BEB) formalism by Bernhardt and Paretzke [18] and Możejko et al. [19], Peudon et al. [20], and Bull et al. [21] using BEB formalism. Huo et al. provided data using an improved binary-encounter dipole (iBED) model [22], and Vinodkumar et al. [23] used a Spherical Complex Optical Potential (SCOP) model and scattering theory. Champion [24] used the Born approximation to calculate the cross sections. The most recent study was by Tan et al. [25], using a semi-empirical approach. The electron ionization induced fragmentation of adenine was studied by Bauer and Grimm [26] using semi-empirical and density functional theory.

Adenine, a purine nucleobase, has a significant role in both protein synthesis and cellular respiration because it is a main component of DNA and ATP. Additionally, adenine is interesting to the astrobiology and astrochemistry community because of the possibility of its formation in space [27–29] and its potential role in the synthesis of larger bio-complexes [30]. Adenine has been found in meteoritic materials [31,32], and a possible precursor of adenine, cyanomethanimine, has been detected in the interstellar medium [33]. Meteorites provide a record of the chemical processes that occurred in the solar system before life began on Earth. Several organic molecular species have been identified so far in astronomical environments, containing the main functional groups necessary to initiate a complex organic chemistry and indicating that many more complex molecules are synthesized in space [34–36]. Until recently, the role of HCN in forming prebiotic molecules in solutions has been speculated [37,38]. However, Chakraborti et al. [27] proposed, on the basis of model calculations, that adenine can be produced in space by HCN oligomerization in the gas phase. Therefore adenine can be viewed as a pentamer of HCN, formed by successive addition of HCN molecules in four steps [39] in gas phase reactions in the dense interstellar clouds in star-forming regions.

Considering the paucity of accurate data, we made extensive measurements on the electron ionization cross sections for DNA bases; total ion cross sections have already been communicated [40]. The only reports on partial cross sections have been by Minaev et al. at 95 eV [11] and by van der Burgt et al. up to 100 eV [16]. Minaev et al. derived the partial cross sections from the total ionization cross sections measured by them, while van der Burgt et al. derived them from theoretical total ionization cross sections. Here, we present the partial ion cross sections by a direct measurement using the relative flow technique up

to the electron energy of 500 eV. We also report ionization energy (IE) for the parent ions and appearance energies (AE) for most fragment ions.

2. Experiment

2.1. Measurement

Accurate determination of target density and the electron current in the interaction volume is needed in a crossed beam experiment to measure the absolute cross sections. It is difficult to determine the target density profile in a beam and its exact volume overlap with the electron beam in the cross-beam experimental set up. This is overcome by a normalization technique called the Relative Flow Technique (RFT) [41], which compares the intensity of the sample species with that of a standard species of known cross section, provided that the measurements for both the gases are carried out under identical experimental conditions. This is achieved by the gas flowing through a capillary under a molecular flow regime so that the molecules effusing out of it will have a specific beam profile independent of the nature of the molecules, and hence the geometry of the interaction volume becomes independent of the nature of the gas. The only change will be a constant multiplier, which depends on the pressure behind the capillary and can be measured accurately. While this technique is rather straightforward for molecules that have enough vapor pressure at room temperature, those with low vapor pressure, especially those that are solids at room temperature, need to be heated to elevated temperatures to increase their vapor pressure. Pressure measurements at such elevated temperatures are technically a very difficult task in cross-beam experimental setups due to the absence of appropriate manometers. The measurements of adenine is one such case. We have overcome this problem by measuring the temperature accurately and using the temperature versus vapor pressure data.

Though the experiment has been described elsewhere [42,43], for completeness we describe the essential features here. It uses an effusive molecular beam formed by a capillary, a magnetically collimated and pulsed electron gun, a Faraday cup to measure the incident electron current, a Time of Flight Mass Spectrometer (ToFMS) to mass select the ions, a pair of micro-channel plates (MCP) in chevron configuration as a detector, and the associated electronics and computer program to record the ion signal as a function of the mass and electron energy.

The effusive beam of adenine molecules is prepared by heating the commercially available sample (Sigma-Aldrich, St. Louis, MO, USA) in the oven to effuse through the capillary directly into the interaction region, as described earlier [43]. The temperature of the oven was gradually increased over a period of a few days to the required value of 474 K, while monitoring the mass spectrum of emanated water vapor. This was to ensure the uniform heating of the sample to thermal equilibrium as well as eliminating the water vapor from the sample. The uniformity of the temperature along the sample was ensured by monitoring it close to both the ends by different well-calibrated thermocouples. The temperature of the sample was maintained at 474 K to obtain reasonable target densities but at a low enough pressure to ensure molecular flow regime. At this temperature, the calculated pressure was 45.82 mTorr, low enough to ensure molecular flow through the capillary (0.2 mm diameter) so that the ratio of mean free path to the capillary diameter was much higher than unity.

The pulsed electron beam was operated at a repetition rate of 5 kHz, with the pulse duration being 300 ns. A pulsed extraction field was applied immediately after the electron pulse to extract the cations resulting from the electron–molecule collisions. The ions were detected by the MCP detector mounted at the end of the flight tube and operated in the pulse counting mode. The ion extraction field and the ion optics, including the flight tube, and the detector biases were optimized to ensure no discrimination in the collection, transmission, and detection of the ions due to the initial velocity distribution of the ions and their mass-to-charge ratio. Uniform detection efficiency was ensured by changing the bias voltage combination on the front and back of the MCP detector plates and looking for relative variation of the intensity of the highest mass peak to that one below 40 amu/e,

and the operating voltages were fixed in the range where this ratio showed saturation. The uniformity of the detector efficiency up to mass-to-charge ratio of 130 amu/e was also confirmed by measuring the positive ion counts on electron impact from Ar and Xe and comparing the ratios of Ar^{2+} to Ar^{+}, Xe^{2+} to Xe^{+}, and Xe^{3+} to Xe^{+} with those reported in the literature. These were found to be in agreement within the experimental uncertainties.

A computer-controlled programming system allowed the storage of the mass spectra, the electron current as a function of the electron energy, and the ion yield curves. The ion yields curves were converted to absolute cross sections by using the Ar^{+} cross section from Argon at 100 eV as the standard. The measurements for Ar were carried out by flowing the gas through the same oven and the capillary tube used for making measurements on the sample molecules. Argon measurements were done immediately before and after under similar experimental conditions, except for the oven temperature. During Ar measurements, the oven was kept at room temperature in order to prevent interference from the adenine sample. An independent set of measurements on argon were carried out at different temperatures to determine any systematic error arising due to higher temperatures. These measurements showed no effect on the argon data with temperature. The pressure of Ar behind the capillary was measured using a capacitance manometer, while the pressure for the sample molecules was determined by using the vapor pressure data of adenine reported by W. Zielenkiewicz [44]. The vapor pressure for adenine at 474 K was determined from the relation [44] given as follows:

$$\log\left(\frac{p}{p0}\right) = 38.4 \pm 0.6 - \frac{17350 \pm 252}{T}$$

In RFT, under identical conditions, we measured the intensities, N_u, of an ion u of the sample gas under study and N_s of an ion of known cross sections, which was used as a standard (s). The partial ionization cross section σ_u can be related with known cross sections (σ_s), as

$$\sigma_u = \sigma_s \times \frac{N_u}{N_s} \times \frac{I_s}{I_u} \times \frac{F_s}{F_u} \times \sqrt{\frac{M_s}{M_u}} \times \frac{K_s}{K_u}$$

where N represents the intensity of each ion, F is the flow rate of individual gases, M is the molecular weight of each gas, and I is the time-averaged electron beam current. K_s and K_u are the efficiency of collection, transmission, and detection of the ion used as the standard and the one under measurement, respectively. This equation can be further simplified, since $F.M^{1/2}$ is proportional to pressure P behind the capillary under molecular flow conditions, as

$$\sigma_u = \sigma_s \times \frac{N_u}{N_s} \times \frac{I_s}{I_u} \times \frac{P_s}{P_u} \times \frac{K_s}{K_u} \quad (1)$$

One of the crucial aspects of the experiment, which was described above, is to ensure that K is the same for all ions so that the ratio K_s/K_u is unity. The possibility of thermal decomposition of adenine was ruled out by measuring the mass spectra at fixed electron energy as a function of temperature over the range of temperature. No change in the relative intensity of the mass spectra or no new fragments were observed with a change in temperature. The possible thermal decomposition of the sample could also be identified by the change of color of the powder on visual inspection of the remaining sample after the experiment. By taking into account all these, we ensured that thermal decomposition did not contribute any erroneous signal in our measurements.

In the measurement procedure, to begin with, the mass spectrum was measured in crossed beam mode at an electron energy of 100 eV and a temperature of 474 K. Next, the ion yield curves for all the fragments were recorded from 0–500 eV. Then, argon was introduced, and Ar^{+} counts were recorded at 100 eV. During the crossed beam measurements the contribution to ion counts coming from the uniformly filled background molecules due to scattering at the surfaces was subtracted from the measured crossed beam data in order to have the contribution from the beam alone. This was done by placing the oven in such a

way that no molecular beam was available in the interaction region and the chamber was filled uniformly by the sample gas. The background mass spectrum was subtracted, and the resultant ion counts were normalized to the electron current and pressure to obtain the normalized counts for each mass fragment. The mass scale was calibrated using Ar^+ and Ar^{++}. Partial cross sections were calculated using Equation (1) given above.

In order to ensure complete collection and detection of the ions, we used voltage biases on the ToF spectrometer, which did not provide the best mass resolution. This resulted in mass peaks overlapping with each other in certain mass ranges, forming a few envelopes. Individual contributions for ions of a given mass-to-charge ratio (m/z) were obtained by unfolding each envelope to individual peaks, assuming Gaussian shapes. The area under each Gaussian was taken as the contribution due to that particular ion.

2.2. Uncertainty Estimation

The uncertainties in the present measurements are estimated as follows. The uncertainties arise from the relative cross section (ion yield curve) measurement as well as from the normalization to the absolute numbers. The uncertainty in the ion yield curves arise mainly from possible overlap volume change (in the electron beam and molecular beam) with respect to the change in electron energy apart from possible variations in the electron current source and target pressure. While strict control could be made in the current source variation and target pressure variation, the systematic error from the volume overlap change is difficult to control. The uncertainty due to temporal variation in the experimental parameters is reduced by completing one scan of the entire electron energy up to 500 eV within 300 s. The reproducibility of the ion yield curves is within 1% over the entire energy range. The volume overlap changes with the electron beam is checked by making measurements on Ar+ from Ar in the electron energy range used here and was consistent with existing data [45] within 5%. Wherever the mass peaks were not clearly resolved, we employ deconvolution, leading to uncertainty in the relative intensities of the peaks thus obtained. The contribution due to this varies depending on the overall shape of the envelopes of peaks and the statistics. In addition to this, uncertainties also arise from measurement of electron current, pressure and statistical errors from ion counting. Non-linear effects due to pulse pile up are addressed by keeping the maximum total count rate (inclusive of all the masses) at the most at one-tenth of the electron beam pulse rate, even though we use a multi-hit card for data acquisition. It is assured that the temperature remains the same at the oven and other end of capillary within 0.1 °C, which causes an uncertainty of less than 0.1% in the vapor pressure. The uncertainty quoted in [44] in the temperature dependence of the vapor pressure data is about 2%, which we assume as the uncertainty in the pressure of adenine. The uncertainty in the Ar pressure measurement is about 0.1%. One important source of uncertainty in the absolute cross sections arises from that of the Ar ionization cross sections we use for normalization. We use the most recent data [45], which quotes an uncertainty of 5%. These data are consistent with other measurements [46–48]. An analysis of the data from all the four sets [45–48] gives a standard deviation of 2.9%. Assuming 5% uncertainty in the Ar data and combining it with the uncertainty in the counting statistics, including that arising from the Gaussian deconvolution of the peaks, pressure measurements and the uncertainty in the ion yield curve provide a total uncertainty of 6% in the present measurements in absolute cross sections for all the ions, which are at least 10% of the intensity of the parent ion. The maximum uncertainty in the detection efficiency for ions over the range of interest is about 10%. This gives a total uncertainty in the cross section measurements of 12%.

3. Results and Discussion

3.1. Mass Spectrum

The relative intensities of the peaks measured at 70 eV and 100 eV electron impact is given in Table 1 along with other reported data. The dominant peaks in the spectrum are $(CNH)_n^+$ with n = 1 to 5 and $HCNH^+$. We could not collect H^+ and measure its intensity

reliably due to the relatively large initial kinetic energy with which it is produced and also due to it getting deflected away during its flight to the detector by the magnetic field used to collimate the electron beam.

Table 1. Relative intensities of major fragment ions from adenine.

m/*z*	Electron Impact						Photon Impact
	Present Work 100 eV	**Minaev et al. [11] 95 eV**	**Present Work 70 eV**	**NIST [50] 70 eV**	**Rice et al. [49] 70 eV**	**Ostroverkh et al. [17] 70 eV**	**Jochims et al. [14] 20 eV**
136	8.0	4.29	8	7.6	-	7.86	-
135	100	100	100	100	100	100	100
134	6	2.86	6.4	3	3	3.32	10
120	0.5	-	0.44	-	3	1.55	1
119	1.3	-	1.3	1.2	-	1.44	3
118	0.8	-	0.81	0.9	-	1.11	-
108	25	35.7	23.7	27	34	30.3	57
107	1.9	5.0	1.8	1.9	3	2.44	10
92	2.4	-	2.4	1.5	-	1.55	9
83	1.3	-	1.2	0.8	-	0.441	-
82	2.0	-	1.9	0.6	-	0.332	-
81	10.2	22.9	9.9	9.7	19	10.9	50
80	5.3	10.0	5.1	3.3	7	4.43	10
70	5.0	5.0	5.0	3.6	5	4.42	17
66	11.8	20.0	11.8	6.3	15	7.59	41
65	3.9	7.14	3.6	1.8	6	2.58	0
56	2.3	-	2.3	1.5	-	1.37	-
55	6.9	11.4	6.6	2.4	-	2.33	-
54	25	32.9	23	11.2	31	15.3	55
53	24	25.7	21	7.6	24	8.45	28
43	7.6	10.0	7.3	4.3	12	6.542	34
42	2.6	5.0	2.3	0.5	3	0.443	16
41	2.7	2.85	2.6	1.1	2	1.03	7
40	6.7	10.0	5.8	1.6	5	1.89	1
39	10.4	10.0	8	2.2	8	2.58	1
38	9.9	11.4	7.2	2.4	10	2.44	0
29	16	8.57	15.5	3.6	12	7.58	60
28	82	21.4	74	18.5	78	67.1	110
27	12.8	10.0	7.7	1.9	12	0.551	10
18	-	-	-	-	-	11.7	-
17	-	-	-	-	-	4.20	-
15	-	-	-	-	-	4.43	-
14	-	-	-	-	-	3.43	-
13	3.9	-	1.5	-	-	-	-
12	2.8	-	0.85	-	-	-	-

The relative intensities measured by Rice and Dudek [49] matches well with our 100 eV electron impact mass spectra within experimental accuracies for most fragments, the notable exceptions being m/z = 54 and 27. The high prominence of the important ion fragment at m/z = 28 observed in the present measurement and in [14,49] is not observed in [11,50]. Recent measurements of van der Burgt [16] also observed relatively high intensity of m/z = 28. Dawley et al. [15] state that the relatively large intensity of m/z = 28 observed by them may due to contamination from N_2. They observed larger intensity for this ion than the parent ion. Considering this, we have tried to eliminate and evaluate the presence of N_2 in our experiment. We eliminate possible external leak from the atmosphere by having a background pressure of a few times 10^{-9} Torr in the experiment. Further, the analysis of the mass spectrum of adenine shows that if at all, there is very little presence of N_2 in our experiment. This is done by looking at the ratio of m/z = 28 to that m/z = 14 (N^+

and N_2^{2+}). The reported value of this ratio at 100 eV from N_2 is 3.2 [51], where as in the present measurements it is about 60. Even assuming that N^+ collection and detection after mass analysis may be skewed due to their relatively large kinetic energy, this ratio is too large. In fact, the measured ratio for N_2^+ to N_2^{2+} (both having thermal energies) from N_2 is about 53 [52]. Our experiment is designed to collect, mass analyze and detect all the ions independent of their initial velocity distribution. We also note the considerable intensity of m/z = 29 (about 20 % of that of m/z = 28), which can only be formed from adenine. Due to its composition, CH_3N^+, its formation needs rearrangement of at least one H atom from another site in the molecule. Even assuming a H atom scrambling may be common place in an excited adenine ion prior to its fragmentation, the probability for the formation of this ion is not too small. Hence the observed high cross section for m/z = 28, which arises from a direct fragmentation process, is not surprising. In view of these we believe that the contribution to m/z = 28 from N_2^+, if at all is very small.

We also observe the ion of m/z = 67.5 with reasonable intensity, which corresponds to doubly charged parent ion, $C_5H_5N_5^{2+}$. We could not obtain a reliable number for its intensity as it is mixed with m/z = 67 and 68 due to limited mass resolution. The ions of m/z = 12 and 13 are also seen in the present data. We note that the low mass ions have relatively higher ion yield in comparison to other experiments. The variation observed in different experiments in the relative intensity of the observed mass peaks may be due to systematic errors in the various experiments. There are two sources of systematic errors that may affect the observed relative ion intensity distribution in the mass spectra. The first one is the variation in efficiency of the detector as a function of the mass-to-charge ratio. The second one is the collection and transmission efficiency of the mass spectrometer. The collection and transmission depend on the initial kinetic energy and angular distribution of the ions. In addition, their mass-to-charge ratio may also come into effect when a quadrupole mass spectrometer is used for mass analysis. The lighter ions are likely to be affected more by the kinetic energy discrimination, while the heavier ions are likely to be affected by the detection efficiencies. In the present measurements, except for the case of H^+, we ensure that the uncertainties due to collection and detection efficiencies are minimized by using narrow electron gun pulses, a large pulsed field extraction and appropriate detector biases, and sensitive pulse counting electronics. Automation of the experiment allowed us to run the experiment without interruption for several days continuously in order to build up adequate statistics while using minimum electron beam current and target pressure. This eliminated various other systematic errors arising from deviation from single collision conditions and detector and counting electronics pile-up issues.

3.2. Appearance Energies and Fragmentation Channels

We measured ion yield curves for most fragment ions from adenine in the energy range 0–500 eV, and the curves near threshold for some prominent ions are shown in Figure 1. The changes in slope of the ion yield curves are indicated by solid lines superimposed on them in order to obtain the appearance energies (AEs). The solid lines were obtained using linear fit. We are unsure whether the exponential fit based on Wannier threshold law is applicable or is critical for determining the appearance energies in the case of ionization of polyatomic molecules due to the absence of well-separated molecular ion states. This becomes particularly troublesome for fragment ion formation from them, as we lack information on the dissociating states and their dynamics. In view of this, we use the relatively simple approach of linear fit. The appearance potentials of the major m/z ions are listed in Table 2, as measured from the onsets in the ion yield curves. The present AE values in this table were derived by reading out the intersection of linear fit with the energy axis. Table 2 also includes the AE measured by Jochims et al. [14] using photon impact and Dawley et al. [15] using electron impact ionization. In most cases, we observed two AE values due to the clear change in the slope of the ion yield curve. Two slopes could be due to the particular ion being formed by two different pathways, with the second one contributing at higher energies. This kind of change of slope in ion yield curve is not apparent in the parent ion

and $C_4H_4N_4^+$ fragment ion (Figure 1). In most ion fragments, our first threshold is in close agreement with the existing measurements using electron impact by Dawley et al. [15].

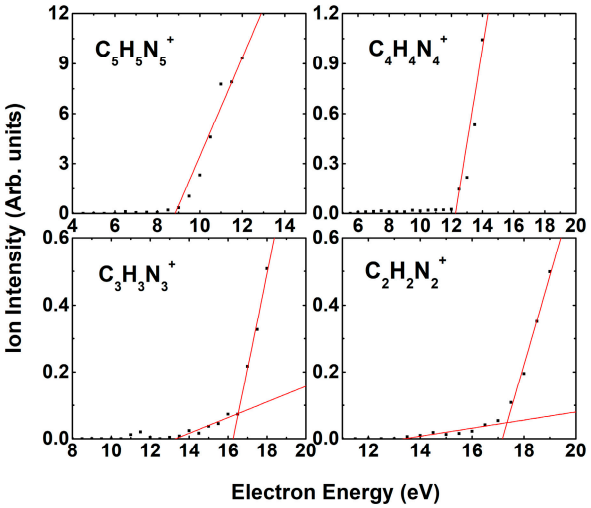

Figure 1. Appearance energies for some major fragment ions from adenine.

Table 2. Appearance energies of major ions from adenine in eV.

m/z	Photon Impact	Electron Impact				
	Jochims et al. [14]	Dawley et al. [15]	van der Burgt et al. [16]	Present		
				1st	2nd	Difference
135	8.2 ± 0.03	8.7 ± 0.3	8.0 ± 0.2	8.8 ± 0.3	-	-
108	11.56 ± 0.05	11.7 ± 0.2	11.3 ± 0.2	12.3 ± 0.5	-	-
94	-	-	-	15 ± 0.5	17 ± 0.5	2
93	-	-	-	15.2 ± 0.5	17.2 ± 0.5	2
92	-	-	-	15.6 ± 0.4	17.6 ± 0.4	2
91	-	-	-	16.5 ± 0.5	-	-
82	-	-	-	15.7 ± 0.4	18.2 ± 0.4	2.5
81	12.8 ± 0.1	14.14 ± 0.5	13.1 ± 0.2	13.5 ± 0.5	16.3 ± 0.5	2.8
80	-	15.1 ± 0.5	14.8 ± 0.7	17.5 ± 0.4	21.5 ± 0.4	4
70	13.1 ± 0.1	14.9 ± 0.2	12.6 ± 0.4	13.0 ± 0.4	16.5 ± 0.4	3.5
66	13.2 ± 0.1	14.2 ± 0.3	13.5 ± 0.2	16.5 ± 0.4	19.0 ± 0.4	2.5
65	-	17.9 ± 0.4	15.7 ± 1.3	17.0 ± 0.4	20.5 ± 0.4	3.5
64	-	-	-	18.5 ± 0.4	-	-
56	-	-	-	16.5 ± 0.4	18.6 ± 0.4	2.1
55	-	-	-	15.5 ± 0.5	18 ± 0.5	2.5
54	13.7 ± 0.1	14.6 ± 0.3	13.5 ± 0.3	13.5 ± 0.5	17.5 ± 0.4	4
53	-	16.7 ± 0.5	15.3 ± 0.5	16.0 ± 0.5	21 ± 0.4	5
51	-	-	-	14 ±0.5	21 ± 0.4	7
43	13.0 ± 0.1	14.0 ± 0.3	13.3 ± 0.6	13.0 ± 0.5	17.0 ± 0.4	4
42	-	-	-	14 ± 0.4	19 ± 0.4	5
41	-	-	-	16 ± 0.4	22 ± 0.4	6
40	-	15.7 ± 0.3	15.9 ± 0.2	16.0 ± 0.5	20.0 ± 0.5	4
39	-	18.1 ± 0.2	17.1 ± 0.5	14.5 ± 0.5	21.5 ± 0.4	7
38	-	-	-	15.0 ± 0.5	23 ± 0.5	8
29	14.0 ± 0.1	15.15 ± 0.15	13.7 ± 0.3	14.5 ± 0.5	-	-
28	13.1 ± 0.1	13.1 ± 0.5	12.9 ± 0.4	15 ± 0.4	17.0 ± 0.4	2

Table 2. *Cont.*

m/*z*	Photon Impact	Electron Impact				
	Jochims et al. [14]	Dawley et al. [15]	van der Burgt et al. [16]	Present		
				1st	2nd	Difference
27	-	13.5 ± 0.2	14.0 ± 0.6	14 ± 0.5	20 ± 0.5	6
25	-	-	-	14 ± 1	-	-
24	-	-	-	15 ± 1	-	-
15	-	-	-	12 ± 0.5	19 ± 0.5	7
14	-	-	-	19.5 ± 0.5	27 ± 0.5	7.5
13	-	-	-	26 ± 1	37 ± 1	11
12	-	-	-	27 ± 1	38 ± 1	11

For the parent ion, m/z = 135 amu, we measured an ionization energy of 8.8 ± 0.3 eV from the ion yield curve shown in Figure 1. This agrees with the 8.8 ± 0.2 eV of Minaev et al. [11] and 8.7 ± 0.3 eV of Dawley et al. [15] both using electron impact ionization and 8.6 ± 0.006 of Plutzer et al. [53] using resonance 2-photon ionization. Our measured value is higher than the 8.2 ± 0.03 of Jochims et al. [14] using photoionization and the vertical ionization energy of 8.08 eV and adiabatic ionization energy of 8.07 eV using quantum chemical calculations by Dawley et al. [15].

The experimental AE value for the formation of m/z = 108 ($C_4H_4N_4^+$) is 12.3 ± 0.5 eV in our work. This AE value matches with that of 12.3 ± 0.1 obtained by Pilling et al. [54] using the photoelectron-photoion coincidence technique (PEPICO) but higher than the 11.56 ± 0.05 eV determined in the photoionization study by Jochims et al. [14] and 11.7 ± 0.2 given by Dawley et al. [15]. Our measured AE value for the formation of m/z = 81 ($C_3H_3N_3^+$) is 13.50 ± 0.5 eV. This is in between the AE value of 14.14 ± 0.5 by Dawley et al. [15] using electron impact and 12.8 ± 0.1 by Jochims et al. using photon impact [14]. We observed an AE value of 13.5 ± 0.5 eV for the formation of m/z = 54 ($C_2H_2N_2^+$). This is close to the AE value of 13.7 + 0.1 by Jochims et al. [14] and lower than the 14.55 ± 0.3 by Dawley et al. [15]. For m/z = 28 ($HCNH^+$) we find the appearance energy to be 15 ± 0.4, which is slightly larger than the values obtained by Jochims [14] and Dawley et al. [15].

We find that a second threshold appears for the formation of fragment ions of m/z = 92 and below. These thresholds should be indicative of new production channels for the respective ions in which the corresponding neutral parts may be fragmenting further. It may also be due to electronic excitation in any of the fragments (ionic or neutral). Additional thresholds for several ions between m/z = 37 and 71 have been observed by van der Burgt et al. [16]. The differences in the first and second thresholds in the present measurements are shown in the last column in Table 2. We note that this difference is about 4 eV or less as we go down in mass, until the production of m/z = 53, which corresponds to $C_2HN_2^+$. The next lower mass we observe is 43, corresponding to $CH_3N_2^+$, which is structurally one less C atom and corresponds to further cleaving of the ring structure. From here on, the difference in the two thresholds increases and reaches as much as 11 eV for C^+ formation, with the notable exception of that of m/z = 28, which is CH_2N^+. This large difference for the lighter ions may also arise from the double ionization process. Since the neutral radicals also play a major role in the chemical reactions in the tracks of high energy radiation, the knowledge of the neutral radical formation plays a crucial role in radiation chemistry. As the detection of neutral fragments are experimentally very difficult, the only method is to model the dissociative ionization process through quantum chemical calculations in order to incorporate these additional channels. In this respect, identification of the higher thresholds may be useful.

The formation mechanism of various ions has been discussed by a number of authors [14–17,26,49,55]. The recent study by Dawley et al. [15] combined experimental results with quantum chemical calculations. The most important aspect of these studies is

the identification of the formation channels for $(CHN)_n^+$ with n = 1 to 4 by elimination of 1 to 4 HCN radicals from the parent $C_5H_5N_5^+$ ion, as shown in Figure 2.

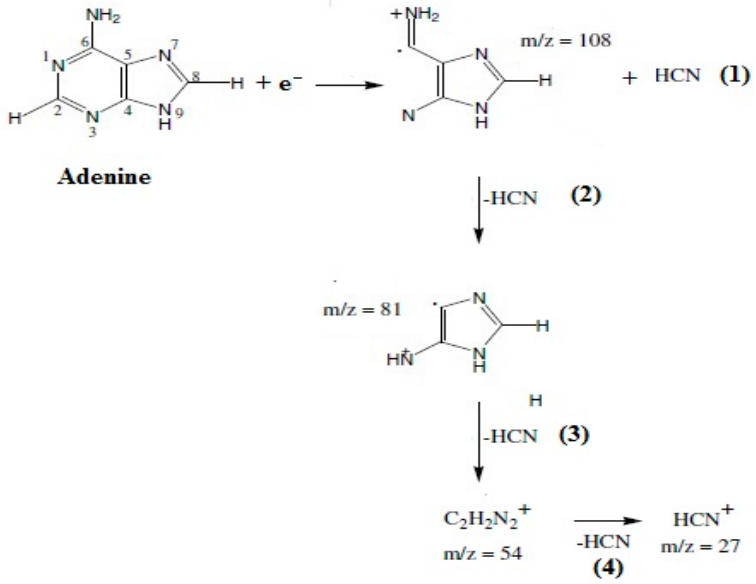

Figure 2. Principal pathway involved in fragmentation of adenine on ionization.

As shown in Table 1, we confirmed prominent fragment peaks corresponding to ions $C_nH_nN_n^+$ (n = 1 to 5) at m/z of 27 (CNH^+), 54 ($C_2N_2H_2^+$), 81 ($C_3N_3H_3^+$), 108 ($C_4N_4H_4^+$), and 135 ($C_5N_5H_5$+) in the mass spectrum of adenine. Each of these ions is formed by the loss of one HCN unit in succession from the adenine molecule. The ratios of partial ionization cross sections for these ions on elimination of HCN units relative to that of the parent ion at 31%, 11.2%, 23%, and 14%, respectively, at 100 eV are considerably high. This is consistent with photoionization [14]. The elimination of HCN is an important process in the electron ionization of polynitrogen heterocycles and constitutes the reaction sequence in many purine derivatives [56], including purine itself [57]. The decomposition of adenine following electron impact has been studied [49,55] on the basis of extensive isotopic substitution to establish the extent of site selectivity in fragment ion formation and by [14] using photon impact to show the successive expulsion of HCN from the adenine. Jochims et al. [14] also show that the corresponding ions $C_nH_nN_n^+$ (n = 1 to 5) have higher relative intensity both in electron and photon impact to adenine. It has been proposed that successive addition of HCN molecules in four steps [39] in gas phase reactions can produce adenine by oligomerization, where it can be seen as a pentamer of HCN [27]. In the fragmentation pattern of adenine, we see that the loss of each unit of HCN leads to a prominent ion with high partial cross sections. Successive loss of HCN is the most preferred pathway, and most ions are formed by losing HCN units in the dissociative ionization of adenine. This could be understood as a de-oligomeriztion of the adenine oligomer by electron impact.

3.3. Cross Sections

Partial cross sections for the formation of all the dominant ions are shown in Figures 3 and 4. In Figure 3, we give the cross sections for the most prominent ions, $(CHN)_n^+$ with n = 1 to 5 and CH_2N^+ (m/z = 28), along with the only other available data for comparison. The partial cross sections for a selected set of prominent ions along with the total cross sections are given in Table 3.

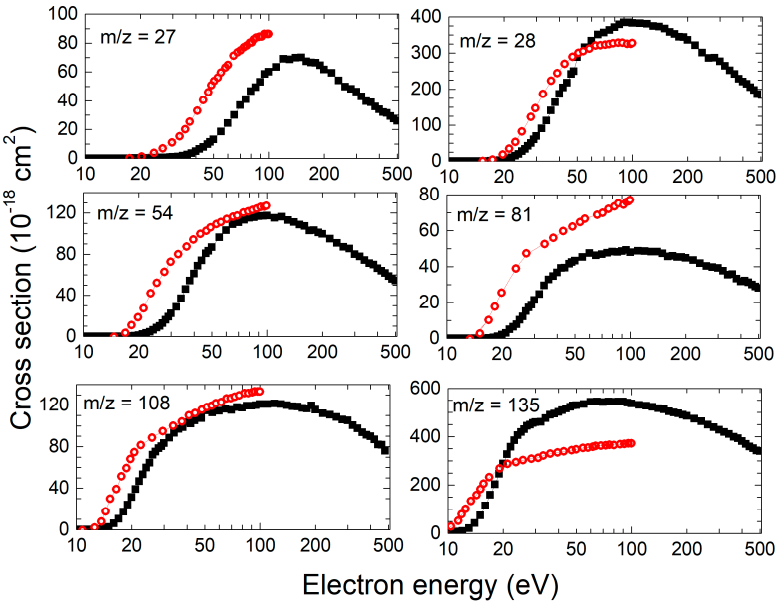

Figure 3. Partial cross sections for formation of $(CHN)_n^+$ (n = 1 to 5) and CH_2N^+. Black filled squares—present data and red open circles—from Ref. [16].

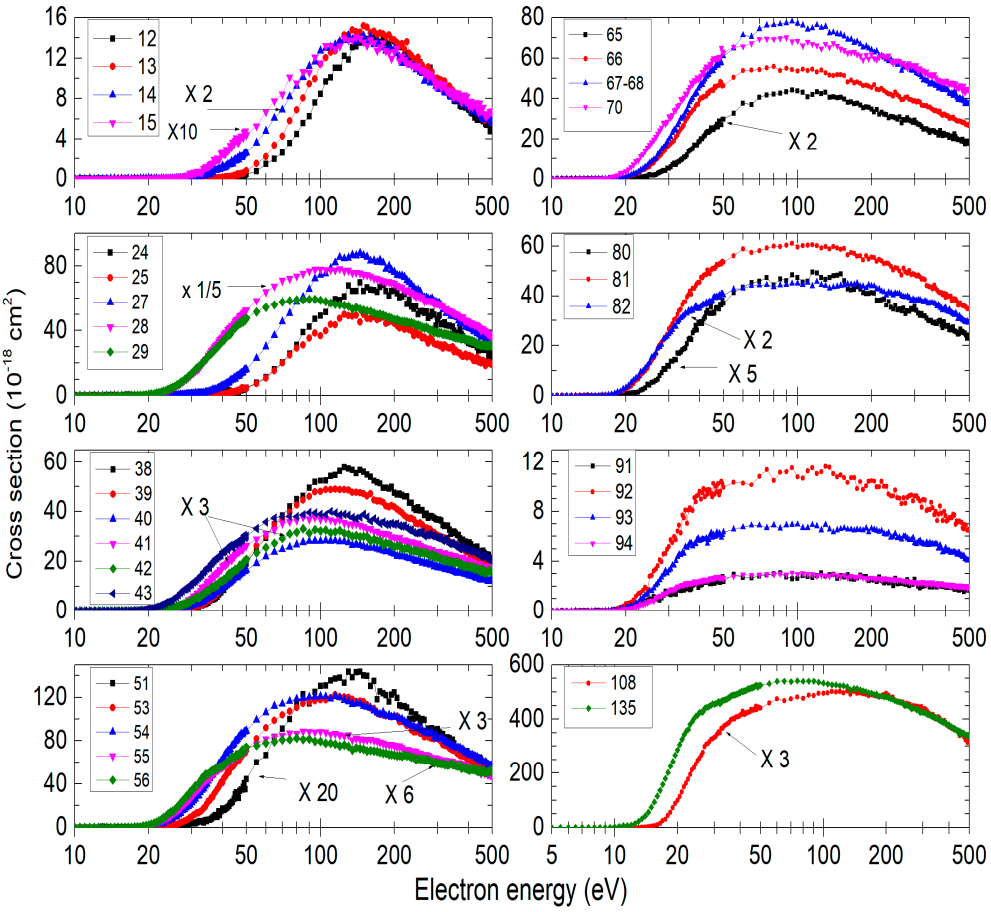

Figure 4. Partial ionization cross sections for all dominant ions from adenine. The numbers in the top left side of the panels represent the m/z values; 67–68 represent three ions of m/z = 67, 67.5, and 68, with 67.5 being the dominant one corresponding to doubly charged parent ion, $C_5H_5N_5^{2+}$.

Table 3. Partial ionization cross sections for prominent ions and the total ion cross section obtained by summing all the partial cross sections.

Electron Energy (eV)	Partial Ionization Cross Sections for Prominent Ions ($\times 10^{-18}$ cm^2)									Total Cross Section (10^{-16} cm^2)
	HCN^+	$HCNH^+$	C_2N^+	C_2NH^+	$C_2N_2H^+$	$C_2N_2H_2^+$	$C_3N_3H_3^+$	$C_4N_4H_4^+$	$C_5N_5H_5^+$	
8.5	0	0	0	0	0	0	0	0	0.20	0.002
9	0	0	0	0	0	0	0	0	0.34	0.003
10	0	0	0	0	0	0	0	0	2.3	0.03
11	0	0	0	0	0	0	0	0	7.8	0.105
12	0	0	0	0	0	0	0	0	9.3	0.138
13	0	0	0	0	0	0	0	0.026	21.7	0.138
14	0	0.025	0	0.015	0	0.01	0.03	0.22	42.9	0.221
15	0	0.05	0.039	0.018	0	0.013	0.04	1.0	74.6	0.407
16	0	0.10	0.070	0.022	0.03	0.02	0.07	2.4	116	0.694
17	0	0.20	0.070	0.032	0.045	0.054	0.22	5.9	159	1.09
18	0	0.73	0.093	0.044	0.12	0.20	0.51	10.4	203	1.53
19	0.079	1.5	0.11	0.059	0.11	0.50	1.2	17.3	246	2.05
20	0.13	3.1	0.23	0.071	0.15	0.97	2.1	24.0	288	2.60
25	0.37	22	0.57	0.25	2.0	8.3	10.4	59.7	418	3.16
30	0.92	65	1.1	1.3	9.1	22.3	21.4	80.3	459	5.93
35	1.8	122	2.9	4.1	22.9	41.4	30.3	93.0	483	8.21
40	4.8	178	7.6	9.2	39.4	61.0	36.7	100	501	10.8
45	8.4	225	12.6	15.7	56.3	77.3	41.1	105	520	12.5
50	13	260	16.9	20.9	68.1	86.8	43.2	107	529	14.4
55	19	289	22.5	26.7	78.7	96.4	45.3	111	535	15.5
60	24	316	26.1	30.5	88.5	103	47.5	115	544	16.9
65	30	334	31.1	35.4	94.7	109	46.3	113	544	18.0
70	37	351	34.2	37.9	99.6	111	46.9	114	542	18.6
75	41	356	37.4	40.2	103	113	47.7	116	545	19.2
80	47	364	40.0	43.1	106	115	48.3	115	543	19.6
85	49	371	41.1	45.3	110	116	48.2	118	544	19.9
90	53	379	44.0	46.7	111	117	48.6	118	544	20.1
95	59	384	46.2	48.5	112	117	49.2	119	540	20.6
100	60	385	46.6	48.8	113	117	48.0	119	536	21.0
125	68	380	51.5	49.4	116	114	47.8	120	527	20.6
150	70	369	49.9	47.8	112	109	47.4	120	512	20.6
175	68	353	45.7	44.8	100	102	45.2	117	495	19.4
200	62	341	42.2	42.4	98.4	99.6	44.8	120	485	19.1
225	58	321	41.0	38.2	90.4	94.1	42.8	113	469	17.0
250	53	305	37.1	35.6	85.5	90.0	41.4	111	455	16.6
275	48	289	33.3	33.5	80.3	84.1	40.1	108	443	16.2
300	46	279	32.6	30.9	79.8	80.1	39.2	105	428	15.3
325	41	264	30.6	28.8	72.4	76.8	37.8	101	418	14.7
350	39	249	28.3	27.4	68.2	73.0	35.2	97.5	405	13.9
375	36	239	25.0	25.4	63.8	69.7	33.6	93.5	391	13.4
400	34	224	23.6	24.3	60.0	66.3	31.8	89.7	381	12.9
425	32	215	22.6	22.6	56.4	64.0	30.8	86.9	368	12.5
450	29	197	20.8	20.2	52.8	58.6	29.2	81.9	346	11.8
475	28	193	20.3	19.8	52.3	57.8	29.0	80.8	347	11.1
500	26	178	18.3	18.9	47.7	54.2	28.1	77.2	340	11.5

From Figure 3, it is apparent that there is considerable difference between the existing data [16] and the present measurements. The difference exists both in magnitude and relative shape of the cross section curves (ion yield curves). The absolute magnitude given in [16] was obtained by normalization with theoretical total ion calculations and hence one may expect some difference. However, the difference in magnitude in the two data sets appears to be beyond this since the differences depend on m/z values. We are unable to attribute the reason for the observed differences except for a possible source of

errors arising from ion transmission efficiencies of the mass spectrometer and detection efficiencies as a function of m/z. As explained in the experimental section, we have taken utmost care in eliminating these errors. The deviations in the shape of the cross section curves in the two measurements should not arise from these errors, at least in the zeroth order. A possible source of error in this respect seems to be overcorrection for the variation in the electron beam current as the current measured at the Faraday cup could be smaller than the actual current passing through the interaction volume. This effect is likely to be more pronounced as the electron energy decreases. As mentioned earlier, we have taken utmost care in eliminating this problem and characterized the experiment satisfactorily using known cross sections.

The complete set of partial ionization cross sections for all the ions of significant intensities are given in Figure 4. As expected, the cross sections for most of the ions rise relatively steeply toward the respective peaks and then decrease rather slowly towards higher energies. The energy corresponding to the cross section peak varies from ion to ion, but with a more or less systematic change as a function of m/z. For example, the peak for the parent ion (m/z = 135) occurs at an energy of about 75 eV, while that for C^+ occurs at about 160 eV. In the panels in Figure 4, we plot the cross sections for bunches of ions, irrespective of their absolute magnitudes, by using appropriate multipliers as given in the panels. This allows comparison of the relative shape of cross section curves within a given mass range, which may provide some insight into their formation process.

Among the ions with m/z = 12 to 15 (C^+, CH^+, N^+ and NH^+), NH^+ has the smallest appearance energy (AE) of 12 eV, followed by N^+ with an AE of 19.5 eV in comparison to CH^+ (AE = 26 eV) and C^+ (AE = 27 eV). That NH^+ has the least AE is not surprising, since it can be formed without breaking either of the two ring structures of adenine. However, it is interesting to note that in terms of absolute cross sections, the overall production of NH^+ is about a factor of 10 smaller than that of CH^+ and C^+ ions. Even the N^+ formation cross section is a factor of 5 higher than that of NH^+.

For the ions of m/z ranging from 24 to 29, we see three different groupings. m/z = 28 and 29 start off earlier than others, with AE of 15 and 14.5 eV respectively. Ion of m/z = 27 (HCN^+) has a yield curve different from others. The third group of m/z = 24 (C_2^+) and 25 (C_2H^+) seem to follow each other, but are different from the other two groups. C_2H^+ and C_2^+ have AEs of 14 eV and 15 eV, respectively. However, the ion yield curves are rather flat, with very small slope at low energies, and do not start rising till about 40 eV for C_2H^+ and 45 eV for C_2^+. HCN^+ has an AE of 18.5 eV and seems to have a second threshold for formation at 30 eV. Possible channels for formation of m/z = 28 ($HCNH^+$) have been discussed by Dawley et al. [15], and they do not favor direct formation through the fragmentation of the imidazole ring based on energetics. However, energy consideration may be valid at the threshold, and beyond the threshold there would be enough excess energy for the parent molecular ion to undergo any sort of structural change leading to fragmentation. The observed similarity in the yield curves of $HCNH^+$ to that of $HCNH_2^+$ (or H_2CNH^+) should help in identifying the fragmentation dynamics leading to these ions. That the $HCNH^+$ formation channel is the most dominant fragmentation channel of adenine ionization demands further study.

In the range of masses 38 to 43, we notice two groups with m/z = 38 and 39 having considerably different shapes for their ion yield curves in comparison to the other four. This difference could be attributed to their composition, which then would have a bearing on the fragmentation of the parent ion. The ions m/z = 38 and 39 would have compositions of C_2N^+ and C_2NH^+, respectively, while those of 40 to 43 would have a composition involving $CN_2H_n^+$ with n varying from 0 to 3. The difference in the number of C and N atoms in the two sets would have a dependence on how the ring structures in adenine break to form the respective fragments. All the ions in these groups of ions have two distinct AEs. As expected, in each of the groups, the AEs keep increasing with the reduction in the number of H atoms.

For the ions of m/z in the range of 51 to 56 also, we can clearly see the dependence of the ion yield curves on the composition of the ions in terms of the number of C, N, and H atoms. By comparing the shapes, one may even distinguish between two likely compositions of a given ion. In this set of ions, we notice three groupings: 51 (which could only be C_3NH^+) (first group), 53 ($C_3NH_3^+$ or $C_2N_2H^+$) and 54 ($C_2N_2H_2^+$) (second group) and 55 ($C_2N_2H_3^+$) and 56 ($C_2N_2H_4^+$) (third group). The ion of m/z = 51 is clearly demarcated from that of 54 with the distinction in the number of C and N atoms, and we see clear difference in the shape of the ion yield curves between the two. The ion of m/z = 53 could have in principle two compositions—$C_3NH_3^+$ or $C_2N_2H^+$. From a comparison of the curve of m/z = 53 with those of 51 and 54, one may conclude that $C_2N_2H^+$ is the most likely composition for 53. The difference between 53 and 54 at low energies and those of 55 and 56 from 54 is indicative of the difference in the number of hydrogen atoms. We note that for an ion with a given number of C and N atoms, the yield curves (and also their peaks) tend to shift to higher electron energies as the number of H atoms decreases. This seems to be the case in almost all the ions we observed.

Next we consider the ions in the range of m/z = 65 to 70. In addition to 65 and 70, we observe 66, 67, 67.5, and 68. The ion of m/z = 67.5 corresponds to the doubly charged parent ion. Due to insufficient mass resolution, we are unable to separate it from m/z = 67 and 68 to obtain accurate numbers. Our analysis shows that at 100 eV, m/z = 68 has very small intensity, and the intensity of m/z = 67.5 is about a factor of three larger in comparison to that of m/z = 68. Thus, the cross section curve identified as m/z = 67–68 may be treated to be mainly that of the doubly charged adenine ion. This may explain the difference in the shape of the curve in comparison to others in the panel. $C_3N_2H^+$ is the composition for m/z = 65, while m/z = 70 is most likely to be $C_2N_3H_4^+$. m/z = 66 has been identified to be $C_3N_2H_2^+$, though, in principle, it could also be $C_2N_3^+$. The yield curves for m/z = 65 and m/z = 70 are clearly different, consistent with their composition and based on what we have seen so far from other groups of ions. The question is, based on the empirical relation we have seen so far, whether we can identify the composition of m/z = 66. We note that the cross section for m/z = 66 peaks at about 80 eV, while that of m/z = 65 ($C_3N_2H^+$) peaks at about 95 eV, and for m/z = 70 ($C_2N_3H_4^+$), it peaks at 90 eV. If m/z = 66 were to be $C_2N_3^+$, its yield curve should have peaked at an energy higher than 90 eV. On the other hand, if its composition is $C_3N_2H_2^+$, its yield curve should peak at an energy smaller than that of m/z = 65 ($C_3N_2H^+$), which it does. So one may conclude that the composition of m/z = 66 is $C_3N_2H_2^+$ and not $C_2N_3^+$. While it may be already known or there may be other means to identify the composition of m/z = 66 from adenine, what we want to show is the consistency in the relation between the composition and the shape of the ion yield curves that we have discussed so far.

In the range of m/z = 80 to 85, we observe three ions, 80, 81 and 82, with 81 ($C_3N_3H_3^+$) being the dominant ion. The yield curve of m/z = 80 is considerably different from the other two. In addition, it has much higher AE (17.5 eV in comparison to 13.5 eV for 81). The mass 80 ion could have two possible compositions. It could be $C_3N_3H_2^+$, that is, one H atom less than that of mass 81 ($C_3N_3H_3^+$), or there could be a difference in the number of C and N atoms along with appropriate number of H atoms, that is, $C_4N_2H_4^+$. Based on the difference in shape of the ion yield curve and the large difference in AE, we may argue that the composition of m/z = 80 is $C_4N_2H_4^+$ and not $C_3N_3H_2^+$.

The cross sections for the ions of m/z = 91 to 94 are relatively low, and their yield curves look almost similar, except for a slight variation in the peak positions. The compositions of the ions are most likely to be $C_4N_3H_n^+$, with n varying from 1 to 4. With only a change in the number of H atoms, it is not surprising to see them having almost similar ion yield curves. The shift in the energy of the peak cross section seems to decrease with an increase in the number of H atoms, consistent with our discussion so far.

We present cross sections for ions of m/z = 108 ($C_4N_4H_4^+$) and 135 (the parent ion, $C_5N_5H_5^+$) in the last panel in Figure 4. As is expected, the ion yield curves for the two look different from each other. The AE of 12.3 $\pm$ 0.5 eV for m/z = 108 is smaller than

all other fragment ions. However, we note that this is slightly larger than other reported measurements [14–16]. The peak cross section for m/z = 108 is at 115 eV. The AE for the parent ion is 8.8 $\pm$ 0.3 eV and is consistent with previous reports. The maximum of the cross section is found to be at about 75 eV. The most notable feature in the case of the parent ion is the presence of some structure in the ion yield curve at about 35 eV.

So far, we have discussed the cross sections in terms of the AEs and the energy corresponding to the peak cross section for given sets of fragment ions. We observed that the lighter the ion, the more the tendency to increase both the AE and the peak energy. In addition, given a fixed number of C and N atoms, the addition of H atoms seems to lower these energies. The general tendency for the lighter ions to have larger peak energy was seen in the case of uracil [43]. This was explained based on the availability of states in the ionization continuum, which increases with electron energy. The shift of the peaks to higher values for lighter ions is due to the fact that these ions have more available channels of formation as compared to the heavier ones. One way this happens is through the opening of multiple ionizations and excitations of heavier ions, which fragments, giving rise to lighter ions.

Figure 5 (reproduced from [40]) shows the total ionization cross sections from threshold to 500 eV. Though already reported, we provide it here for continuity and as a marker of accuracy for the partial cross sections. As mentioned earlier, the absolute total cross sections were obtained by summing the absolute partial ion cross sections that we measured. Thus, total ion cross sections would indicate the accuracy of the measured partial ion cross sections. In the figure, our total ion cross sections are compared with the available experimental [11,16] and theoretical results [18–24]. So far, only Minaev et al. [11] have made absolute cross section measurements for adenine up to 200 eV. Their results are considerably larger than the present results and all the theoretical results. As mentioned earlier, van der Burgt et al. [16] measured the relative cross sections up to 100 eV and normalized them to absolute values using the average value of various theoretical results at 70 eV. All theoretically calculated cross section curves exhibit the typical shape, with a maximum energy between 80–90 eV and a gradual decline towards higher energies. The cross sections in our measurements peak at 100 eV. On the whole, there is reasonable agreement between our data and most of the theoretical results. However, it appears that the improved binary-encounter dipole (iBED) model employed by Huo et al. [22] provides the best agreement. We also note that the recent calculations by Tan et al. [25] (not shown in the figure) have better agreement with the present results below 100 eV. Very recently, Mendez et al. [58] provided a scaling rule for the ionization of biological molecules by fully stripped ions. Their scaling law for H^+ projectiles and our results for electron projectiles show excellent agreement for adenine along with other DNA bases. This is important in the context of the limited electron impact data with which we could compare the present results. The consistency shown in the scaling behavior indirectly certifies the accuracy of the present total ion cross sections and, consequently, the present partial ion cross sections.

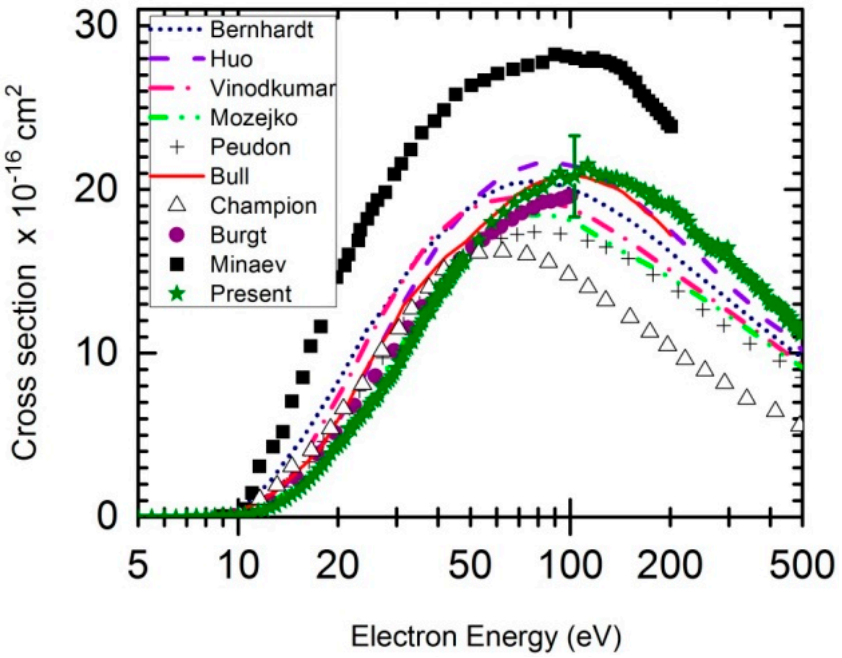

Figure 5. Total ionization cross section for the adenine molecule and its comparison with the existing data (Reproduced from Ref. [40]).

4. Conclusions

In this work, we used a crossed electron-molecular beam experiment along with the Relative Flow Technique (RFT) to measure the absolute partial ionization cross sections of adenine molecules, which exist in solid form at room temperature. The total ionization cross sections obtained from summing the partial cross sections are compared with the theoretical calculations and are found in reasonable agreement. Our measured cross section values are in close agreement with the theoretical calculation by Huo et al. [22] using the improved binary-encounter dipole (iBED) model. The relative ion intensities (mass spectrum) and appearance energies measured are also found in reasonable agreement with the existing data. The most abundant fragment cations from adenine include $C_nH_nN_n^+$ (n = 5, 4, 3, 2, 1) at m/z of 135 ($C_5N_5H_5$+), 108 ($C_4N_4H_4^+$), 81 ($C_3N_3H_3^+$), 54 ($C_2N_2H_2^+$), 27 (CNH^+), and $HCNH^+$ as determined from the experiment. The dominance of $C_nH_nN_n^+$ (n = 1 to 5) confirmed by our cross section measurements shows that the most thermodynamically favored pathway for adenine dissociation due to electron ionization appears to be the loss of HCN molecules in succession. This supports the idea of formation of adenine by successive addition of HCN units and may help us in understanding the formation of adenine in space.

Comparison of the ionization yield curves for various sets of fragment ions provided some interesting, though not unexpected results. We find that lighter ions tend to have higher appearance energies as well as higher energies at which the cross section peaks. Within a group of ions with a given number of C and N atoms, we find that there is a systematic shift in the abovementioned energies as a function of the number of H atoms. We also find that we are able to use this information to identify the composition of a given ion where more than one possibility exists. The fact that adenine is a relatively simple system with only three species of atoms was helpful in this respect. It would be interesting to investigate this idea in other similar molecules. Rich possibilities exist for the further investigation of dissociative ionization of adenine using momentum imaging. Finally, we hope that the measured partial cross sections will be immediately useful in biochemical modelling and Monte Carlo track simulations to understand the damage mechanism in the living cells and in other applications.

Author Contributions: Conceptualization of the experiment: E.K. Method and measurements: carried out by M.A.R. under the guidance of E.K. Analysis of the data and preparation of the manuscript: all authors. All authors have read and agreed to the published version of the manuscript.

Funding: This research received no external funding.

Institutional Review Board Statement: Not applicable.

Informed Consent Statement: Not applicable.

Data Availability Statement: Data are contained within the article.

Conflicts of Interest: The authors declare no conflict of interest.

References

1. Ward, J.F.; Webb, C.F.; Limoli, C.L.; Milligan, J.R. *Ionizing Radiation Damage to DNA: Molecular Aspects*; Wiley-Liss: New York, NY, USA, 1990; p. 43.
2. Huels, M.A.; Hahndorf, I.; Illenberger, E.; Sanche, L. Resonant dissociation of DNA bases by subionization electrons. *J. Chem. Phys.* **1998**, *108*, 1309–1312. [CrossRef]
3. Boudaõffa, B.; Cloutier, P.; Hunting, D.; Huels, M.A.; Sanche, L. Resonant Formation of DNA Strand Breaks by Low-Energy (3 to 20 eV) Electrons. *Science* **2000**, *287*, 1658–1660. [CrossRef] [PubMed]
4. Hunniford, C.A.; McCullough, R.W.; Jeremy, R.; Davies, H.; Timson, D. DNA damage by low-energy ions. *Biochem. Soc. Trans.* **2009**, *37*, 893–896. [CrossRef]
5. Baccarelli, I.; Bald, I.; Gianturco, F.A.; Illenberger, E.; Kopyra, J. Electron-induced damage of DNA and its components: Experiments and theoretical models. *Phys. Rep.* **2011**, *508*, 1–44. [CrossRef]
6. Nikjoo, H.; Neill, P.O.; Terrissol, M.; Goodhead, D.T. Quantitative modelling of DNA damage using Monte Carlo track structure method. *Radiat. Environ. Biophys.* **1999**, *38*, 31–38. [CrossRef] [PubMed]
7. Rabus, H.; Nettelbeck, H. Nanodosimetry: Bridging the Gap to Radiation Biophysics. *Radiat. Meas.* **2011**, *46*, 1522–1528. [CrossRef]
8. Nettelbeck, H.; Rabus, H. Nanodosimetry: The missing link between radiobiology and radiation physics? *Radiat. Meas.* **2011**, *46*, 893–897. [CrossRef]
9. Schardt, D.; Elsasser, T.; Schulz-Ertner, D. Heavy-ion tumor therapy: Physical and radiobiological benefits. *Rev. Mod. Phys.* **2010**, *82*, 383. [CrossRef]
10. Shafranyosh, I.I.; Sukhoviya, M.I. Inelastic collisions of the uracil molecules with electrons. *J. Chem. Phys.* **2012**, *137*, 184303–184306. [CrossRef]
11. Minaev, B.F.; Shafranyosh, M.I.; Svida, Y.Y.; Sukhoviya, M.I.; Shafranyosh, I.I.; Baryshnikov, G.V.; Minaev, V.A. Fragmentation of the adenine and guanine molecules induced by electron collisions. *J. Chem. Phys.* **2014**, *140*, 175101. [CrossRef] [PubMed]
12. Shafranyosh, I.I.; Sukhoviya, M.I.; Shafranyosh, M.I. Absolute cross sections of positive- and negative-ion production in electron collision with cytosine molecules. *J. Phys. B.* **2006**, *39*, 4155–4162. [CrossRef]
13. Shafranyosh, I.I.; Sukhoviya, M.I.; Shafranyosh, M.I.; Shimon, L.L. Formation of positive and negative ions of thymine. *Tech. Phys.* **2008**, *53*, 1536–1540. [CrossRef]
14. Jochims, H.W.; Schwell, M.; Baumgartel, H.; Leach, S. Photoion mass spectrometry of adenine, thymine and uracil in the 6–22 eV photon energy range. *Chem. Phys.* **2005**, *314*, 263–282. [CrossRef]
15. Dawley, M.M.; Tanzer, K.; Cantrell, W.A.; Plattner, P.; Brinkmann, N.R.; Scheier, P.; Denifl, S.; Ptasinska, S. Electron ionization of the nucleobases adenine and hypoxanthine near the threshold: A combined experimental and theoretical study. *Phys. Chem. Chem. Phys.* **2014**, *16*, 25039–25053. [CrossRef] [PubMed]
16. van der Burgt, P.J.M.; Finnegan, S.; Eden, S. Electron impact fragmentation of adenine: Partial ionization cross sections for positive fragments. *Eur. Phys. J. D* **2015**, *69*, 173. [CrossRef]
17. Ostroverkh, A.; Zavilopulo, A.; Shpenik, O. Ionization of guanine, adenine and thymine molecules by electron impact. *Eur. Phys. J. D* **2019**, *73*, 38. [CrossRef]
18. Bernhardt, P.H.; Paretzke, H.G. Calculation of electron impact ionization cross sections of DNA using the Deutsch–Märk and Binary–Encounter–Bethe formalisms. *Int. J. Mass Spectrom.* **2003**, *223–224*, 599–611. [CrossRef]
19. Możejko, P.; Sanche, L. Cross section calculations for electron scattering from DNA and RNA bases. *Radiat. Environ. Biophys.* **2003**, *42*, 201–211. [CrossRef] [PubMed]
20. Peudon, A.; Edel, S.; Terrissol, M. Molecular basic data calculation for radiation transport in chromatin. *Radiat. Prot. Dosim.* **2006**, *122*, 128–135. [CrossRef]
21. Bull, J.N.; Lee, J.W.L.; Vallance, C. Absolute electron total ionization cross-sections: Molecular analogues of DNA and RNA nucleobase and sugar constituents. *Phys. Chem. Chem. Phys.* **2014**, *16*, 10743–10752. [CrossRef] [PubMed]
22. Huo, W.M.; Dateo, C.E.; Fletcher, G.D. Molecular data for a biochemical model of DNA damage: Electron impact ionization and dissociative ionization cross sections of DNA bases and sugar-phosphate backbone. *Radiat. Meas.* **2006**, *41*, 1202–1208. [CrossRef]
23. Vinodkumar, M.; Limbachiya, C.; Barot, M.; Swadia, M.; Barot, A. Electron impact total ionization cross sections for all the components of DNA and RNA molecule. *Int. J. Mass Spectrom.* **2013**, *339–340*, 16–23. [CrossRef]

24. Champion, C. Quantum-mechanical predictions of electron-induced ionization cross sections of DNA components. *J. Chem. Phys.* **2013**, *138*, 184306. [CrossRef] [PubMed]
25. Tan, H.Q.; Mi, Z.; Bettiol, A.A. Simple and universal model for electron-impact ionization of complex biomolecules. *Phys. Rev. E* **2018**, *97*, 032403. [CrossRef]
26. Bauer, C.A.; Grimme, S. Elucidation of electron ionization induced fragmentations of adenine by semiempirical and density functional molecular dynamics. *J. Phys. Chem. A* **2018**, *118*, 11479. [CrossRef] [PubMed]
27. Chakraborti, S.; Chakraborti, S.K. Can DNA bases be produced during molecular cloud collapse? *Astron. Astrophys.* **2000**, *354*, L6–L8.
28. Saladino, R.; Crestini, C.; Costanzo, G.; Negri, R.; di Mauro, E. A possible prebiotic synthesis of purine, adenine, cytosine, and 4(3H)-pyrimidinone from formamide: Implications for the origin of life. *Bioorg. Med. Chem.* **2001**, *9*, 1249–1253. [CrossRef]
29. Gupta, V.P.; Tandon, P.; Rawat, P.; Singh, R.N.; Singh, A. Quantum chemical study of a new reaction pathway for the adenine formation in the interstellar space. *Astron. Astrophys.* **2011**, *528*, A129. [CrossRef]
30. Evans, N.L.; Ullrich, S.; Bennett, C.J.; Kaiser, R.I. On the interaction of adenine with ionizing radiation: Mechanistical studies and astrobiological implications. *Astrophys. J.* **2011**, *730*, 69. [CrossRef]
31. Callahan, M.P.; Smith, K.E.; Cleaves, H.J.; Ruzicka, J.; Stern, J.C.; Glavin, D.P.; House, C.H.; Dworkin, J.P. Carbonaceous meteorites contain a wide range of extraterrestrial nucleobases. *Proc. Natl. Acad. Sci. USA* **2011**, *108*, 13995. [CrossRef]
32. Martins, Z.; Botta, O.; Fogel, M.L.; Sephton, M.A.; Glavin, D.P.; Watson, J.S.; Dworkin, J.P.; Schwartz, A.W.; Ehrenfreund, P. Extraterrestrial nucleobases in the Murchison meteorite. *Earth Planet. Sci. Lett.* **2008**, *270*, 130–136. [CrossRef]
33. Zaleski, D.P.; Seifert, N.A.; Steber, A.L.; Muckle, M.T.; Loomis, R.A.; Corby, J.F.; Martinez, O.; Crabtree, K.N.; Jewell, P.R.; Hollis, J.M.; et al. Detection of E-cyanomethanimine toward Sagittarius B2(N) in the Green Bank telescope primos survey. *Astrophys. J. Lett.* **2013**, *765*, L10. [CrossRef]
34. Stoks, P.G.; Schwartz, A.W. Uracil in carbonaceous meteorites. *Nature* **1979**, *282*, 709–710. [CrossRef]
35. Joyce, G.F. The antiquity of RNA-based evolution. *Nature* **2002**, *418*, 214–221. [CrossRef]
36. Ziurys, L.M. The chemistry in circumstellar envelopes of evolved stars: Following the origin of the elements to the origin of life. *Proc. Natl. Acad. Sci. USA* **2006**, *103*, 12274–12279. [CrossRef] [PubMed]
37. Oro, J.; Kimball, A.P. Synthesis of purines under possible primitive earth conditions: II. Purine intermediates from hydrogen cyanide. *Arch. Biochem. Biophys.* **1962**, *96*, 293–313. [CrossRef]
38. Sanchez, R.A.; Ferris, J.P.; Orgel, L.E. Studies in prebiotic synthesis. IV. Conversion of 4-aminoimidazole-5-carbonitrile derivatives to purines. *J. Mol. Biol.* **1968**, *38*, 121–128. [CrossRef]
39. Volkenshtein, M.V. *Biophysics*; Mir Publishers: Moscow, Russia, 1983.
40. Rahman, M.A.; Krishnakumar, E. Communication: Electron ionization of DNA bases. *J. Chem. Phys.* **2016**, *144*, 161102. [CrossRef]
41. Srivastava, S.K.; Chutjian, A.; Trajmar, S. Absolute elastic differential electron scattering cross sections in the intermediate energy region. I. H_2. *J. Chem. Phys.* **1975**, *63*, 2659–2665. [CrossRef]
42. Rahman, M.A.; Gangopadhyay, S.; Limbachiya, C.; Joshipura, K.N.; Krishnakumar, E. Electron ionization of NF_3. *Int. J. Mass Spectrom.* **2012**, *319–320*, 48–54. [CrossRef]
43. Rahman, M.A.; Krisnakumar, E. Absolute partial and total electron ionization cross sections of uracil. *Int. J. Mass Spectrom.* **2015**, *392*, 145. [CrossRef]
44. Zielenkiewicz, W.J. Enthalpies of Sublimation and Vapor Pressures of Adenine, 1-Methyladenine, 2-Methyladenine, 3-Methyladenine, and 8-Methyladenine. *Chem. Eng. Data* **2000**, *45*, 626. [CrossRef]
45. Rejoub, R.; Lindsay, B.G.; Stebbings, R.F. Determination of the absolute partial and total cross sections for electron-impact ionization of the rare gases. *Phys. Rev. A* **2002**, *65*, 042713. [CrossRef]
46. Krishnakumar, E.; Srivastava, S.K. Ionisation cross sections of rare-gas atoms by electron impact. *J. Phys. B At. Mol. Opt. Phys* **1988**, *21*, 1055–1082. [CrossRef]
47. Straub, H.C.; Renault, P.; Lindsay, B.G.; Smith, K.A.; Stebbings, R.F. Absolute partial and total cross sections for electron-impact ionization of argon from threshold to 1000 eV. *Phys. Rev. A* **1995**, *52*, 1115–1124. [CrossRef]
48. Ma, C.; Sporleder, C.R.; Bonham, R.A. A pulsed electron beam time of flight apparatus for measuring absolute electron impact ionization and dissociative ionization cross sections. *Rev. Sci. Instrum.* **1991**, *62*, 909–924. [CrossRef]
49. Rice, J.M.; Dudek, G.O. Mass spectra of nucleic acid derivatives. **II.** Guanine, adenine, and related compounds. *J. Am. Chem. Soc.* **1967**, *89*, 2719–2725. [CrossRef]
50. Data Compiled by: NIST Mass Spectrometry Data Center, Wallace, W.E. Adenine Mass Spectrum (Electron Ionization). Available online: https://webbook.nist.gov/cgi/cbook.cgi?ID=C73245&Units=SI&Mask=200#Mass-Spec (accessed on 1 September 2015).
51. Krishnakumar, E.; Srivastava, S.K. Cross sections for the production of N_2^+, N^++N_2^{2+} and N^{2+} by electron impact on N_2. *J. Phys. B At. Mol. Opt. Phys.* **1990**, *23*, 1893–1903. [CrossRef]
52. Mark, T.D. Cross section for single and double ionization of N_2 and O_2 molecules by electron impact from threshold up to 170 eV. *J. Chem. Phys.* **1975**, *63*, 3731–3736. [CrossRef]
53. Plutzer, C.; Kleinermanns, K. Tautomers and electronic states of jet-cooled adenine investigated by double resonance spectroscopy. *Phys. Chem. Chem. Phys.* **2002**, *4*, 4877–4882. [CrossRef]
54. Pilling, S.; Lago, A.F.; Coutinho, L.H.; de Castilho, R.B.; de Souza, G.G.B.; de Brito, A.N. Dissociative photoionization of adenine following valence excitation. *Rapid Commun. Mass Spectrom.* **2007**, *21*, 3646–3652. [CrossRef] [PubMed]

55. Sethi, S.K.; Gupta, S.P.; Jenkins, E.E.; Whitehead, C.W.; Townsend, L.B.; McCIoskey, J.A. Mass spectrometry of nucleic acid constituents. Electron ionization spectra of selectively labeled adenines. *J. Am. Chem. Soc.* **1982**, *104*, 3349–3353. [CrossRef]
56. Porter, Q.N.; Baldas, J. *Mass Spectrometry of Heterocyclic Compounds*; Wiley-Interscience: New York, NY, USA, 1971.
57. Goto, T.; Tatematsu, A.; Matsuura, S. Organic mass spectrometry. I. Mass spectra of pteridine, methylpteridines, and hydroxypteridines. *J. Org. Chem.* **1965**, *30*, 1844–1846. [CrossRef]
58. Mendez, A.M.P.; Montanari, C.C.; Miraglia, J.E. Scaling rules for the ionization of biological molecules by highly charged ions. *J. Phys. B At. Mol. Opt. Phys.* **2020**, *53*, 175202. [CrossRef]